$(TiO_4)^-$ in alpha -quartz studied by low-temperature electron paramagnetic resonance

1992 J. Phys.: Condens. Matter 4 4063

(http://iopscience.iop.org/0953-8984/4/15/019)

J. Phys.: Condens. Matter 4 (1992) 4063–4073. Printed in the UK

$[TiO_4]^-$ in α-quartz studied by low-temperature electron paramagnetic resonance

Phillip Bailey†, Thomas Pawlik‡, Hubert Söthe‡, Johann-Martin Spaeth‡ and John A Weil†

† Department of Chemistry, University of Saskatchewan, Saskatoon, SK, S7N 0W0, Canada

‡ Fachbereich Physik, Universität-GH Paderborn, Warburger Strasse 100A, W-4790 Paderborn, Federal Republic of Germany

Received 11 December 1991

Abstract. The centre $[TiO_4]^-$, formed by x-irradiation at 77 K in naturally occurring crystalline rose quartz, has been studied by single-crystal electron paramagnetic resonance (EPR) spectroscopy. Here the central $3d^1Ti^{3+}$ ion exists within a slightly distorted oxygen tetrahedron. The hyperfine matrix of the low-abundance isotope ^{49}Ti was measured at 8 K and the **g** matrix was measured at several temperatures from 30 K down to 4 K. The analysis of the spin-population distribution within the centre showed that the unpaired spin is almost entirely in the Ti 3d orbital $|3z^2 - r^2\rangle$. Estimates of the spin–lattice relaxation time T_1 and of the EPR linewidth in the temperature range 4–30 K were also obtained. T_1 decreases exponentially with increasing temperature, presumably owing to phonon coupling to the low-lying excited state $|xy\rangle$ which is 8.1 meV (65 cm^{-1}) above the ground state, via an Orbach process. At temperatures above approximately 15 K, the abnormally large EPR linewidth is predominantly caused by lifetime broadening through T_1. The near degeneracy of $|3z^2 - r^2\rangle$ and $|xy\rangle$ indicate that $[TiO_4]^-$ has almost tetrahedral symmetry.

1. Introduction

The study of point defects in crystalline quartz using electron paramagnetic resonance (EPR) spectroscopy has been reviewed (Weil 1984). Certain ions, including Al^{3+} and Ti^{4+}, are thought to substitute for Si^{4+}. The type of paramagnetic species generated after x-irradiation of quartz depends on the temperature of irradiation and subsequent treatment. X-irradiation at or below about 77 K removes electrons from donor centres, e.g.

$$[AlO_4/M]^0 \xrightarrow{h\nu} [AlO_4/M]^+ + e^-$$

(where M ≡ H, Li, Na, etc). The electrons thus liberated transfer to acceptor centres. In the present work we deal with the centre $[TiO_4]^-$ generated from the acceptor centre $[TiO_4]^0$. The anionic species is a rare example of a (nearly) tetrahedral species containing a $3d^1$ ion (Isoya and Weil 1979). It is unstable above 100 K, acting as an acceptor for an ion M^+. It exhibits a relatively large EPR linewidth (about 0.3 mT at 25 K) for a defect centre in quartz; the origin of the broadening was not clear.

0953-8984/92/154063+11$04.50

Until now only the matrix **g** of this centre had been measured, at 25 K, and only a few ^{47,49}Ti hyperfine signals at certain angles had been observed, which did not allow even an approximate fitting of the titanium hyperfine matrices (Isoya and Weil 1979). A better understanding of $[TiO_4]^-$ compared with the well-analysed charge-compensated $[TiO_4/M]^0$ centres seemed desirable and led us to carry out further studies, reported herein.

2. Experimental details

The same crystal reference-axis system is employed herein as in previous publications (Nuttall and Weil 1981, Mombourquette *et al* 1986). The Cartesian axes x, y and z where $x \equiv a_1$, $z \equiv c$ and $y \boxminus z \otimes x$, will be used in this discussion. The orientation of the static magnetic field B relative to the crystal threefold axis c, and to the axis a_1 (crystal twofold axes $a_i \perp c, i = 1,2,3$) is given by polar angle $\theta =< (c, B)$, and azimuthal angle $\phi =< (a_1, c \otimes B \otimes c)$. For our purposes (θ, ϕ) is equivalent to $(\pi - \theta, \pi + \phi)$. In our work, the crystal rotation was approximately about one twofold axis, defined to be a_1 (figure 1).

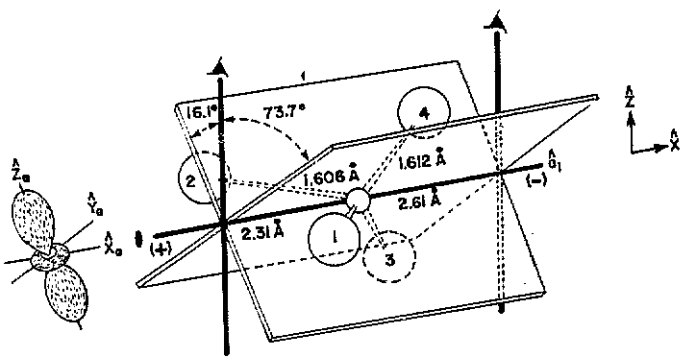

Figure 1. The TiO_4 tetrahedron in crystalline quartz for the uncompensated $[TiO_4]^-$ centre, with the unpaired-electron Ti 3d orbital shown on the left. The larger open circles represent the oxygen ions. The coordinate system is described in the text.

In pure α-quartz, each silicon ion is located (time average) on a twofold axis in a slightly distorted tetrahedral environment. There are two different bond lengths from oxygen ions to the central silicon (or defect) ion. The proper rotation group of α-quartz, which controls the magnetic symmetry-related sites observable by EPR, is D_3 (see figure 1). Any defect centre of local symmetry C_1 is found in any one of six symmetry-related differently oriented sites (labelled $1, 1', 2, 2', 3$ and $3'$) for this crystal symmetry (Weil 1984). The sites i and i′ are interrelated by 180° rotation about a_i. The six EPR spectra reduce to three when $B \perp a_1$ (since the spectra from the site pairs $(1,1')(2,3')$ and $(3,2')$ become superimposed), and to one when $B \| c$. Centres of C_2 symmetry display three distinct symmetry-related sites (1, 2, 3) at general orientations of B, two sites (1, with 2 and 3 spectra superimposed) when $B \perp a_1$, and one site (1, 2, 3 superimposed) when $B \| c$.

A sample (15 mm × 4.4 mm × 1.5 mm) of Brazilian rose quartz was used in the present study. The sample was first thermally bleached at 650 K for 6 h before

transfer to the spectrometer. No EPR signals could be detected down to 4 K. At 77 K the crystal was then x-irradiated, using a Philips MCN101 tube operating at 60 kV and 15 mA *in situ*, for 60 min with no warm-up during and after irradiation.

The EPR spectra were taken using a custom-built computer-controlled EPR–ENDOR spectrometer (Söthe 1989) capable of operation with sample temperatures between 3.5 and 340 K (±0.5 K). The temperature is controlled using a carbon–glass resistor which is mounted into the body of the cold cavity. The quartz crystal was glued to the sample holder so that, within ±2°, $B \perp a_1 \| B_1$ (CW, linearly polarized microwave magnetic field) with crystal rotation (approximately) around the axis a_1.

The main-line spectrum of $[TiO_4]^-$ at 30 K was measured first, at 5° intervals over a 180° rotation. The computer program EPR.FOR was used to perform weighted non-linear least-squares fitting of the line positions to the angles θ and ϕ, utilizing the $[TiO_4]^-$ **g** matrix known at this temperature (Isoya and Weil 1979). The sample orientation obtained in this way was verified by recording the spectrum of the well-known $[AlO_4/Li]^+$ centre also present (Nuttall and Weil 1981).

The program EPR.FOR was then used to perform weighted non-linear least-squares fitting of the 30 K spectral line-position data to parameter matrices, via exact numerical diagonalizations of the spin-Hamiltonian matrix. Each peak was given a weighting factor, dependent on the certainty with which its position could be measured, with a default weighting factor of 1. The program also yielded and utilized the deviation of the rotation axis from a_1. The actual axis was at $\theta = 91.4°$, $\phi = 359.7°$. Subsequent crystal rotations about this axis yielded spin-Hamiltonian parameters at 8 and 4 K.

3. Experimental results

3.1. Spin-Hamiltonian parameters

Parameter matrices were determined for the same spin-Hamiltonian.

$$\mathcal{H} = \beta_e S\cdot(\mathbf{g}_i)\cdot B + \sum_j [S\cdot(\mathbf{A}_j)\cdot I_j - \beta_n I_j\cdot(g_{nj})_i \cdot B + I_j\cdot(\mathbf{P}_j)_i \cdot I_j] \qquad (1)$$

as described previously (Weil 1984), where the index j runs over the nuclei with $I > 0$, i.e. ^{47,49}Ti. All parameter matrices in (1) were taken to be symmetric, with g_{nj} taken to be isotropic in each case and will be given herein for site type $i = 1$.

For $[TiO_4]^-$ at 30 K, the g-value at $B\|c$ is 1.9832(1) and the linewidth from the main lines due to the spinless titanium isotopes is 0.3 mT. The line positions could be measured to an accuracy of ±0.03 mT, which limits the accuracy of the **g**-matrix elements to ±0.0002. The **g** matrices quoted in this work are those derived from fitting of the main-line positions, unless otherwise stated. The low-abundance stable isotopes of titanium with non-zero nuclear spin are ^{47}Ti ($I = \frac{5}{2}$; $g_n = -0.315\,39$; $|e|Q = 4.64 \times 10^{-48}$ C m^2; natural abundance, 7.4%) and ^{49}Ti ($I = \frac{7}{2}$; $g_n = -0.315\,477$; $|e|Q = 3.84 \times 10^{-48}$ C m^2; natural abundance, 5.4%). The values of g_n for the isotopes are so similar that the hyperfine matrices cannot be obtained separately for $[TiO_4]^-$, because of its relatively large linewidth. Hence the EPR parameters for ^{49}Ti only were calculated. The matrix **A**(^{47}Ti) can be calculated from the relation **A**(^{47}Ti) $\simeq 0.999\,72$**A**(^{49}Ti). For $[TiO_4]^-$ at 8 K, the g-value at $B\|c$ is 1.9850(1) and the (calculated) ^{49}Ti hyperfine splitting is 0.83(6) mT. Figure 2 shows an example of the EPR spectra obtainable. The Ti hyperfine lines are very

weak (see figure 2(*b*)) in comparison with the central line. The hyperfine lines could not be measured within approximately $\pm 15°$ of $B \| c$ for any site, because of overlapping between lines. This resulted in relatively large uncertainties in the ^{49}Ti matrix element zz (table 2). The spin-Hamiltonian parameters thus determined are collected in tables 1 and 2.

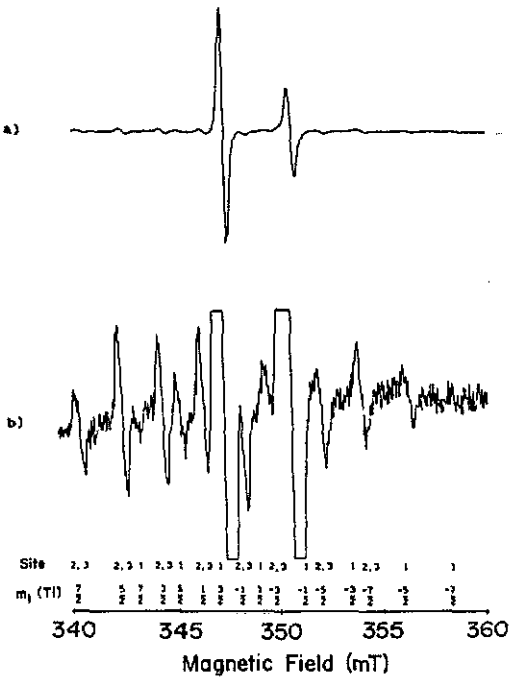

Figure 2. EPR spectrum of $[TiO_4]^-$ at 8 K, $\nu \simeq 9.41$ GHz, $\theta = 108.42°$ and $\phi = 91.30°$ showing: (*a*) the main lines from spinless titanium isotopes (signals due to sites $(2, 2', 3, 3')$ on left and sites $(1, 1')$ on right) and (*b*) the less intense signals due to the $^{47,49}Ti$ isotopes (30x scale of (*a*)).

3.2. Spin–lattice relaxation and EPR linewidth

At very low temperatures the EPR lines are narrow and their shape is Lorentzian, indicating that they are homogeneously broadened. This is consistent with the failure to see any ENDOR lines of neighbouring atoms. (Note that the nearest-neighbour oxygen atoms are 99.99% $^{16,18}O$, which have no nuclear moments.) $[TiO_4]^-$ is thus an 'isolated' centre formed by replacement of Si^{4+} by Ti^{3+}. At 4.4 K, for example, the peak-to-peak linewidth of the first derivative of the unsaturated EPR line is 0.016 mT (site 1; $\theta = 352°$). This linewidth corresponds to a transverse spin–spin relaxation time T_2 of 5×10^{-7} s.

It was noted that in order to measure the unsaturated EPR lines the microwave power had to be very much attenuated at low temperatures. For example, at 6 K, saturation effects became apparent already for a microwave power incident on the cavity of 0.35 μW (the quality factor of the cylindrical cavity was about 7000 in the TE_{011} mode). Upon raising the temperature, the microwave power required to saturate the EPR line became larger and larger, following an exponential temperature dependence. In figure 3 the logarithm of the microwave power needed to observe incipient saturation effects is shown as a function of inverse temperature. For each temperature the relative decrease in the EPR signal intensity from the linear dependence on microwave power was taken to be the same. The unsaturated EPR signals

Table 1. Spin-Hamiltonian parameter matrix **g** for $[TiO_4]^-$ at various temperatures, with statistical error estimates. The last figure in the g-factors (**g**-matrix) is uncertain to 1–2 units.

Matrix **g**			Principal value		Principal directions (deg)	
			k	g_k	θ_k	ϕ_k
			30 K			
1.9240	0	0	1	1.9909	19.71(5)	90
	1.9391	0.0218	2	1.9249	90	0
		1.9831	3	1.9223	70.29(5)	270
Number of angles, 37; number of data points, 74; sum of weighting parameters, 49.34; RMSD of magnetic-field line positions, 0.046 mT						
			8 K			
1.9251	0	0	1	1.9932	19.95(4)	90
	1.9280	0.0235	2	1.9251	90	0
		1.9848	3	1.9195	70.05(4)	270
Number of angles, 37; number of data points, 74; sum of weighting parameters, 67.07; RMSD of magnetic-field line positions, 0.049 mT						
			4 K			
1.9240	0	0	1	1.9920	19.80(3)	89.9(1)
	1.9269	0.0234	2	1.9240	90.10(2)	179.6(6)
		1.9836	3	1.9185	70.20(3)	269.5(7)
Number of angles, 28; number of data points, 164; sum of weighting parameters, 121.7; RMSD of magnetic-field line positions, 0.055 mT						

depend linearly on the microwave power. Since saturation is due to the longitudinal spin–lattice relaxation time T_1 as seen from the saturation factor $\gamma^2 B_1^2 T_1 T_2$ in the Bloch equations (Pake and Estle 1973) the data shown in figure 3 indicate that T_1 follows an exponential temperature-dependence form

$$T_1^{-1} \propto \exp(-C/T) \tag{2}$$

with $C = 97 \pm 2$ K, which is equivalent to an activation energy of 65 cm^{-1}. An exponential temperature dependence of T_1 is characteristic of an Orbach process in which the ground-state Zeeman levels are phonon coupled to an excited state of the defect (see, e.g. Al'tshuler and Kosyrev 1974). Thus our saturation measurements disclose that $[TiO_4]^-$ has a low-lying excited state at 65 ± 2 cm^{-1}. We shall show below that this state is a low-lying Ti 3d orbital.

Up to about 14 K the EPR linewidth is determined by T_2. Above approximately 16–18 K the linewidth increases exponentially with increasing temperature with the same activation energy as found for the saturation behaviour (see full line in figure 4). Thus, at a sufficiently high temperature, the linewidth is determined by T_1. At higher temperatures the unusually large linewidth is caused by a lifetime broadening arising from the fast spin–lattice relaxation events due to the Orbach process.

4. Discussion

The principal values Y_1, Y_2 and Y_3 of any 3×3 symmetric matrix **Y** can conveniently

Table 2. Spin-Hamiltonian parameter matrices $\mathbf{Y} = \mathbf{A}'(^{49}\mathrm{Ti})$ and $\mathbf{P}'(^{49}\mathrm{Ti})$ for $[TiO_4]^-$ at 8 K, with statistical error estimates. The matrix **g** was kept constant at the value calculated at 8 K (table 1). Number of angles, 32; number of data points, 249; sum of weighting parameters, 189.6; RMSD of magnetic-field line positions: with **P** included, 0.070 mT; with **P** excluded, 0.077 mT. Matrix $\mathbf{A}'(^{47}\mathrm{Ti}) \simeq 0.99972\ \mathbf{A}'(^{49}\mathrm{Ti})$. Matrix $\mathbf{P}'(^{47}\mathrm{Ti}) \simeq 21Q(^{47}\mathrm{Ti})/[10Q(^{49}\mathrm{Ti})]\mathbf{P}'(^{49}\mathrm{Ti})$.

Matrix **Y**			Principal value		Principal directions (deg)	
			k	Y_k	θ_k	ϕ_k
		With **P'** included				
A'(^{49}Ti)(mT)						
2.101(12)	0	0	1	−0.127(40)	20.4(3)	90
	1.819(9)	−0.722(17)	2	2.087(12)	69.6(3)	270
		0.141(36)	3	2.101(12)	90	0
P'(^{49}Ti)(mT)						
−0.053(5)	0	0	1	0.083(5)	5(2)	90
	−0.029(4)	0.010(5)	2	−0.030(4)	85(2)	270
		0.082(5)	3	−0.053(5)	90	0
		With **P'** excluded				
A'(^{49}Ti)(mT)						
2.152(6)	0	0	1	−0.400(40)	21.4(3)	90
	1.808(10)	−0.867(10)	2	2.148(6)	68.6(3)	270
		−0.059(40)	3	2.152(6)	90	0

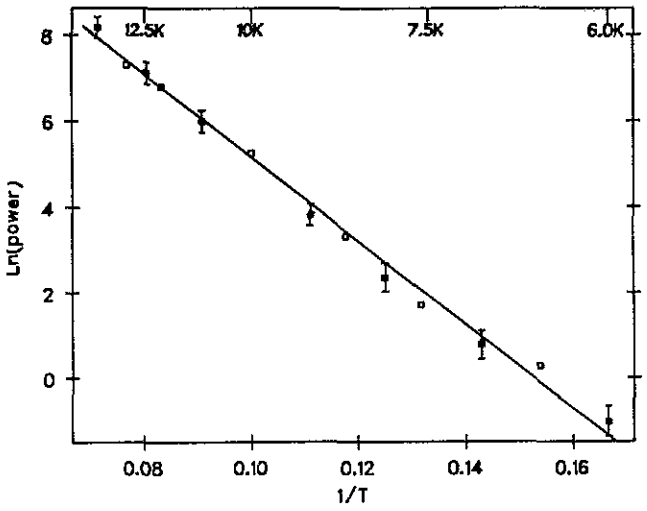

Figure 3. Temperature dependence of the saturation behaviour of the EPR lines. The logarithm of the power needed for incipient saturation is plotted against the reciprocal temperature (see text).

be described by three components: the isotropic component $a = (Y_1 + Y_2 + Y_3)/3$, the uniaxial component $b = (Y_1 - a)/2$, where Y_1 is the value farthest from a and the asymmetry parameter $c = |Y_2 - Y_3|/2$. When hyperfine matrices are given in units of milliteslas, they will be denoted herein by **A'**. For example $\mathbf{A}' = (10^3\mathrm{mT}/T)\mathbf{A}/g_e\beta_e$, where g_e is the free-electron g-value and β_e is the Bohr magneton.

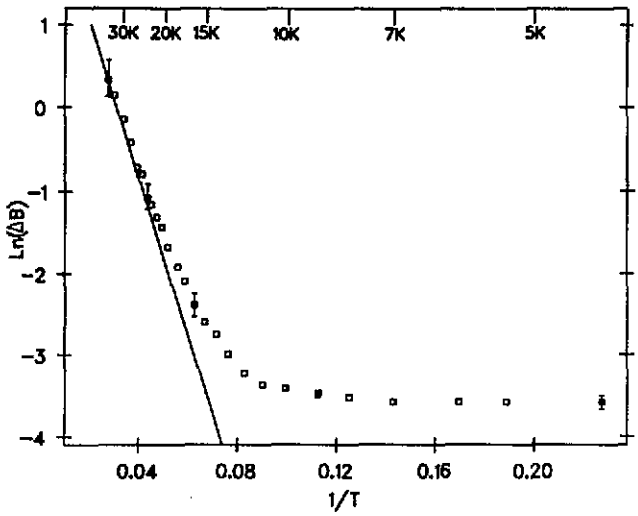

Figure 4. Temperature dependence of the EPR linewidth as a function of temperature. The logarithm of the peak-to-peak linewidth of the first-derivative EPR line is plotted against the reciprocal temperature.

4.1. Matrix **g**

The matrix **g** measured at 30 K was found to exhibit only minor differences compared with the measurements made at 25 K previously (Isoya and Weil 1979). The isotropic component of **g** was found to be 1.9458(2) at 30 K while at 4 K a value of 1.9448(2) was obtained. As noted previously (Isoya and Weil 1979), the principal g-directions are close to the directions bisecting the O–Si–O angles in crystalline quartz, which are given respectively by θ, $\phi = (16.1, 90°)$, $(90, 0°)$ and $(73.7, 270°)$ at about 290 K. The matrices **g** for 30, 8 and 4 K are given in table 1.

4.2. Matrices **A**(^{49}Ti) *and* **P**(^{49}Ti) *and excited-states analysis*

The titanium hyperfine lines were detected using 64.5 kHz modulation amplitude (about 0.3 mT) and a relatively high microwave power (about 0.1 mW at 8 K). These conditions, chosen such that the line intensities were large enough for precise determination of the field positions but low enough that line-broadening saturation effects only just started to appear (so that these did not affect the determination of the line positions). Parameter matrices were separately fitted to the hyperfine line positions at 8, 15 and 30 K. Only minor changes in the matrices were found over this temperature range. Since the largest data set was available at 8 K, decreasing the statistical errors in the hyperfine and quadrupole matrices derived, only the 8 K data (table 2) will be considered.

For $[TiO_4]^-$ the principal (approximately uniaxial) direction with the largest principal value of the matrix **A** (^{49}Ti) was found to be perpendicular to the crystal twofold axis, as also is the case in the lithium and sodium charge-compensated centres (Isoya *et al* 1988, Bailey and Weil 1992). In comparison with the charge-compensated centres, the other principal directions of **A**(^{49}Ti) of $[TiO_4]^-$ exhibit a 180° difference in ϕ, with θ approximately unchanged (±7°). This difference in principal directions will be considered below. We note that matrices **g** and **A** (^{49}Ti) are very close to being coaxial.

The inclusion of matrix **P**(^{49}Ti) in our data fitting is debatable. As seen from table 2, its matrix elements exhibit statistical errors indicating it to be meaningful but marginally so. The principal values are of the same magnitude as those found for $[TiO_4/H]^0_A$ (Rinneberg and Weil 1972). Exclusion of **P** does not affect matrix **A** (^{49}Ti) in any significant fashion (table 2).

The isotropic component a' of **A**(^{49}Ti) has a value of 1.35(4) mT at 8 K, whereas in the charge-compensated centres $[TiO_4/Li]^0_A$, $[TiO_4/Na]^0_A$ and $[TiO_4/H]^0_A$ the values are 1.279 mT, 1.722 mT and 0.928 mT respectively (Isoya *et al* 1988, Bailey and Weil 1992, Rinneberg and Weil 1972). The sign of a' was chosen by taking b' to be negative, the latter in accordance with the negative sign of g_n. Thus we find that a' and b' have opposite signs. In $[TiO_4]^-$, $b'_{expt} = -0.74(4)$ mT and $c'_{expt} = 0.007(12)$ mT. Thus **A** (^{49}Ti) is close to uniaxial. The theoretical uniaxial component value

$$b'_{3d} = \mu_0 g g_n \beta_n \langle r^{-3} \rangle_{3d} \alpha / 4\pi g_e \tag{3}$$

for a pure Ti 3d orbital was estimated to be −0.72 mT (Isoya *et al* 1988). Here α is the d-type spherical-harmonic factor $\langle (1 - 3\cos^2\theta)/2 \rangle$, which has the value $\frac{2}{7}$ for d_{z^2}. Comparison of b'_{expt} with b'_{3d} shows that virtually all the unpaired electron spin population in $[TiO_4]^-$ is located in the Ti d orbitals.

The following somewhat more quantitative analysis of matrix **A**(^{49}Ti), yielding an exact fit of matrices **g** and **A**(^{49}Ti) in terms of a d-orbital admixture, is made with the approximation that the centre exhibits C_{2v} symmetry, i.e. a tetrahedron distorted along the twofold axis a_1 (figure 1). The method of analysis used herein was originally proposed (Banks *et al* 1967, McGarvey 1969) for the study of the $3d^1$ Cr^{5+} species CrO_4^{3-} in Ca_2PO_4Cl. It is convenient to define a new Cartesian coordinate system x_a, y_a, z_a (as shown in figure 1). Considering an SiO_4 unit in crystalline quartz, we take x_a along a_1, z_a in the plane containing the average of the bisectors of O(2)–Si–O(4) and O(1)–Si–O(3) ($\theta = 16.1°$, $\phi = 90°$), and $y_a = z_a \otimes x_a$ (about 1° from the plane containing the average of the bisectors of O(1)–Si–O(4) and O(2)–Si–O(3) ($\theta = 73.7°$, $\phi = 270°$)). Axes y_a and z_a would be twofold symmetry axes if the differences in the O–Si–O bond angles and in the Si–O bond lengths were absent.

In cubic symmetry, the orbitals $|3z_a^2 - r_a^2\rangle$ and $|x_a y_a\rangle$ are degenerate and for tetrahedral symmetry are the lowest-energy d orbitals. For C_{2v} symmetry, $|3z_a^2 - r_a^2\rangle$ and $|x_a^2 - y_a^2\rangle$ have the same A_1 symmetry label and thus may be mixed by the non-cubic parts of the crystalline potential, whereas $|x_a y_a\rangle$ does not mix with any other d orbital. It can be shown (Rinneberg and Weil 1972) that the ground-state wavefunction of the unpaired electron may be expressed as

$$|0\rangle = c_1|3z_a^2 - r_a^2\rangle + c_2|x_a^2 - y_a^2\rangle. \tag{4}$$

We assume that all the unpaired-spin population is located in the d orbitals of titanium, i.e. that $|c_1|^2 + |c_2|^2 = 1$. Fitting to **g** and **A** yields values (table 3) for c_1 and c_2 as well as an approximate value of the hyperfine anisotropy parameter $P_{3d} = g_e \beta_e b'_{3d}/\alpha$ and of the energies of three of the 3d-orbital excited states relative to $|0\rangle$. The data were initially fitted using constant estimated values of the spin–orbit coupling $\lambda = 154$ cm^{-1} and $P_{3d}/hc = -23.61 \times 10^{-4}$ cm^{-1} (Isoya *et al* 1988), and then using the same λ with P_{3d} as an additional variable parameter. The initial estimate of P_{3d} proved reasonable, as only a small change of about 5% was found in P_{3d} when it was included as a variable to produce an exact fit of matrices **g** and

A. Only the values obtained with the fixed value of P_{3d} are shown in table 3. The parameter

$$K = -(A_{x_a} + A_{y_a} + A_{z_a} + [(g_e - g_{x_a}) + (g_e - g_{y_a}) + (g_e - g_{z_a})]P_{3d})/3 \qquad (5)$$

represents the isotropic hyperfine interaction due to core polarization (Rinneberg and Weil 1972). The values of the fitted parameters for the centres $[TiO_4/Li]^0_A$ (Isoya *et al* 1988) and $[TiO_4/Na]^0_A$ (Bailey and Weil 1992) have been included in table 3 for comparison.

Table 3. Mixing coefficients of d orbitals and spectroscopic parameters for $[TiO_4]^-$ and two charge-compensated titanium centres. Replace axes x_a, y_a, z_a with x', y', z' for the charge-compensated centres. Here $x'(=x)$ is along a_1 and y' in the internuclear short-bonded oxygen direction. Vector $z' = y' \otimes x'$ (about 1° from the internuclear long-bonded oxygen direction) as shown in figure 1 of Isoya *et al* (1988). This is the axis system utilized by Isoya *et al* (1988) and by Bailey and Weil (1992).

	$[TiO_4]^-$	$[TiO_4/Li]^0_A$ [a]	$[TiO_4/Na]^0_A$ [b]
Temperature (K)	8	35	35
c_1	0.999	0.874	0.903
c_2	0.031	−0.485	−0.429
$\Delta E_{x_a y_a}/hc$ (cm^{-1})	130	4.070	4.480
$\Delta E_{y_a z_a}/hc$ (cm^{-1})	11 540	13 640	12 470
$\Delta E_{z_a x_a}/hc$ (cm^{-1})	11 550	13 970	11 780
P_{3d}/hc (10^{-4} cm^{-1})	−23.61	−23.61	−23.61
K/hc (10^{-4} cm^{-1})	−11.32	−10.55	−14.63
A_{x_a}/hc, experimental (10^{-4} cm^{-1})	19.64	5.847	11.401
A_{x_a}/hc, calculated (10^{-4} cm^{-1})	20.16	5.134	10.918
A_{y_a}/hc, experimental (10^{-4} cm^{-1})	19.51	24.330	28.802
A_{y_a}/hc, calculated (10^{-4} cm^{-1})	20.00	25.909	30.224
A_{z_a}/hc, experimental (10^{-4} cm^{-1})	−1.187	5.854	8.084
A_{z_a}/hc, calculated (10^{-4} cm^{-1})	−2.119	4.988	7.145

[a] Data from Isoya *et al* (1988).
[b] Data from Bailey and Weil (1992).

In $[TiO_4]^-$ the admixture into $|0\rangle$ of the $|x_a^2 - y_a^2\rangle$ d orbital is small, whereas in $[TiO_4/Li]^0_A$ and $[TiO_4/Na]^0_A$ the admixture is appreciable (table 3). The difference between $g_{z_a} = 1.9932$ (table 1; 8 K data) and g_e is due to the distortion from uniaxial symmetry of the unpaired-electron distribution, implying that the small observed difference (table 3) between A_{x_a} and A_{y_a} is real and that the admixture of $|x_a^2 - y_a^2\rangle$ is significant, but very small. Note that the values of b' for centres $[TiO_4/Li]^0_A$ and $[TiO_4/Na]^0_A$ (+0.66 mT (Isoya *et al* 1988) and +0.68 mT (Bailey and Weil 1992) respectively) are positive, i.e. opposite to that of $[TiO_4]^-$. This presumably is the result of the substantial admixture of $|x_a^2 - y_a^2\rangle$. Using the above treatment of an admixture for d orbitals in $[TiO_4]^-$ yielded results similar to those (Banks *et al* 1967, McGarvey 1969) for CrO_4^{3-}. The deviation from tetrahedral symmetry in both $[TiO_4]^-$ and CrO_4^{3-} is small, as evidenced by the fact that the $|x_a y_a\rangle$ orbital (which is degenerate with $|3z_a^2 - r_a^2\rangle$ in tetrahedral symmetry) is found at a low energy above $|0\rangle$ in both species. The relaxation behaviour of $[TiO_4]^-$ is very similar to that of CrO_4^{3-} (Van Reijen *et al* 1963).

Evidence for a low-energy excited state was also presented in section 3.2, where the spin–lattice relaxation via an Orbach process indicated the existence of an excited

state about 65 cm^{-1} above $|0\rangle$. It is obvious that we should identify this excited state as the low-lying $|x_a y_a\rangle$ orbital. The analysis of the **g** and **A** matrices and the analysis of the temperature dependence of the spin–lattice relaxation time consistently yield the existence of a low-lying excited 3d state. The precision of the determination of its energy position is much higher from the temperature dependence of T_1 since its values depend very sensitively on the activation energy. The analysis of the principal values of the **g** matrix yields only value for the ratio $\lambda/\Delta E_{x_a y_a}$. To derive $\Delta E_{x_a y_a}$ in table 3, the free-ion value of λ was utilized. This does not take into account any covalency effects of either the ground state or excited states. These effects are expected to reduce λ appreciably. Typically reductions of 30% or more can result (Stoneham 1985, Moreno 1991). In view of this and the uncertainty in determining the energy of the excited states from such small deviations from g_e of the three principal values of the **g** matrix and because the simple crystal-field model was used for the analysis, the agreement of the energy position of the excited $|x_a y_a\rangle$ state as derived from the **g** matrix with that derived from T_1 is satisfactory. Thus $|x_a y_a\rangle$ is almost degenerate with $|3z_a^2 - r_a^2\rangle$, i.e. the deviation from tetrahedral symmetry in $[TiO_4]^-$ is very small. We see from table 3 that the values of P_{3d} and K are much the same for all three titanium centres. It follows that there are no major differences in the spin distribution, except in orientation. In $[TiO_4]^-$ there is an angular offset (about 44°) about the twofold axis of the principal directions compared with those in the titanium charge-compensated centres.

In the simple crystal-field model (Banks *et al* 1967, McGarvey 1969), used to analyse the matrix $\mathbf{A}(^{49}Ti)$, the effect of the oxygen lone pairs of electrons present in $[TiO_4]^-$ was neglected. The C_{2v} approximation, ignoring other neighbouring atoms, will presumably be most severe in the analysis of the compensated centres, which shows relatively larger deviations from tetrahedral symmetry than does $[TiO_4]^-$. However, despite the much larger approximations inherent in modelling the compensated centres, the theoretical results there do appear to account reasonably well for the experimental observations (table 3).

5. Conclusions

The present work indicated that $[TiO_4]^-$ has very close to tetrahedral symmetry and that its unpaired electron is predominantly located in a titanium $|3z^2 - r^2\rangle$ 3d orbital. The calculated d-orbital energy levels and orbital mixing coefficients along with the spin–lattice relaxation behaviour disclose the presence of a very low-lying $|xy\rangle$ state and are qualitatively similar to those for another known $3d^1$ tetrahedral species: CrO_4^{3-}. However, the deviation from tetrahedral symmetry is considerably smaller in $[TiO_4]^-$, indicated since $|3z^2 - r^2\rangle$ and $|xy\rangle$ are almost degenerate. The addition of an interstitial charge-compensating cation to $[TiO_4]^-$ results in substantial changes in the orientation of the unpaired-electron distribution within the centre but maintains the total spin population in the Ti 3d orbitals.

Acknowledgments

This work was supported by the Natural Sciences and Engineering Research Council of Canada, and by the University of Saskatchewan. We thank P Alteheld and M J Mombourquette for their assistance.

References

Al'tshuler S A and Kosyrev B M 1974 *Electron Paramagnetic Resonance in Compounds of Transition Elements* (New York: Wiley) p 179
Bailey P and Weil J A 1992 *J. Phys. Chem. Solids* **53** 309
Banks E, Greenblatt M and McGarvey B R 1967 *J. Chem. Phys.* **47** 3772
Isoya J, Tennant W C and Weil J A 1988 *J. Magn. Reson.* **79** 90
Isoya J and Weil J A 1979 *Phys. Status Solidi* a **52** K193
McGarvey B R 1969 *Electron Spin Resonance of Metal Complexes* ed Teh Fu Yen (New York: Plenum) p 1
Mombourquette M J, Tennant W C and Weil J A 1986 *J. Chem. Phys.* **85** 68
Moreno M 1991 private communication
Nuttall R H D and Weil J A 1981 *Can. J. Phys.* **59** 1709
Pake G E and Estle T L 1973 *The Physical Principles of Electron Paramagnetic Resonance* (Reading, MA: Benjamin) p 41
Rinneberg H and Weil J A 1972 *J. Chem. Phys.* **56** 2019
Söthe H 1989 *Doctoral Dissertation* Universität-Gesamthochschule, Paderborn, Federal Republic of Germany
Stoneham A M 1985 *Theory of Defects in Solids* (Oxford: Clarendon) section 13.1
Van Reijen L L, Cossee P and Van Haren H J 1963 *J. Chem. Phys.* **38** 572
Weil J A 1984 *Phys. Chem. Minerals* **10** 149